R. & M. No. 2165
(5592)
A.R.C. Technical Report

MINISTRY OF SUPPLY

AERONAUTICAL RESEARCH COUNCIL
REPORTS AND MEMORANDA

Experiments on Laminar-flow Aerofoil EQH 1260 in the William Froude National Tank and the 13 ft. x 9 ft. and the 9 ft. x 7 ft. Wind Tunnels at the National Physical Laboratory

By

A. FAGE, A.R.C.S. and W. S. WALKER,
of the Aerodynamics Division, N.P.L.

LONDON: HIS MAJESTY'S STATIONERY OFFICE
1948
Price 3s. 6d. net

Experiments on Laminar-flow Aerofoil EQH 1260 in the William Froude National Tank and the 13ft. × 9ft. and 9ft. × 7ft. Wind Tunnels at the National Physical Laboratory

By

A. FAGE, A.R.C.S. and W. S. WALKER,
of the Aerodynamics Division, N.P.L.

Reports and Memoranda No. 2165

January, 1942

Summary.—Reason for Enquiry.—To determine whether the flow conditions in the William Froude National Tank and the new 13 ft. × 9 ft. and 9 ft. × 7 ft. tunnels at the National Physical Laboratory are sufficiently steady to allow the properties of laminar-flow aerofoils to be investigated at high Reynolds numbers: and to obtain information on the behaviour of laminar-flow aerofoil section EQH 1260.

Range of Investigation.—Experiments were made for the following conditions:—

	Chord	Aspect ratio	Range of Reynolds numbers covered. Millions	Experiment
The William Froude National Tank				
Wax model	10 ft.	0·5	4·6 to 7·7	Measurement of drag for median section by pitot-traverse method. Incidence 0 deg.
9 ft. × 7 ft. Tunnel				
Wooden model.—(i) spanning tunnel from floor to roof.	42 in.	Infinite	1·1 to 4·3	Drag and pressure distribution for median section of each model. Incidence 0 deg. Pressure distributions for sections 0·214*c* from the median sections of models (ii) and (iii).
(ii) with round ends	42 in.	0·548	1·1 to 4·3	
(iii) with square ends	42 in.	0·5	1·1 to 4·3	
13 ft. × 9 ft. Tunnel				
(i) Wooden model spanning tunnel from floor to roof.	70 in.	Infinite	1·8 to 8·2	Drag for median section. Incidence 0 to 4·5 deg.
(ii) Wooden model covered with metal skin.	70·4 in.	Infinite	1·6 to 6·9	Drag for median section. Incidence 0 deg.
(iii) Wooden model spanning tunnel from floor to roof.	42 in.	Infinite	1·8 to 5·1	Drag for median section. Incidence 0 deg.

Calculations of profile drag for the section at 0 deg. incidence were made for Reynolds numbers 10^6, $3{\cdot}162 \times 10^6$, 10^7 and for transition points at 0·24, 0·49 and 0·74 of the chord.

Conclusions.—(i) The 13 ft. × 9 ft. and the 9 ft. × 7 ft. tunnels are suitable for the investigation of the properties of laminar-flow aerofoils at Reynolds numbers up to about 5 millions.

(ii) The William Froude National Tank cannot be used to investigate the properties of laminar-flow aerofoils at high Reynolds numbers unless an experimental technique can be devised for which disturbances, due to surface wave and eddy formation, do not matter.

(iii) The lowest value of C_{D_0} obtained, 0·0030, is that measured at a Reynolds number 5·4 millions on metal-skin model, $c = 70{\cdot}4$ in., in the 13 ft. × 9 ft. tunnel. The rise in C_{D_0} beyond this Reynolds number is very steep and the measurements of C_{D_0} in this region are indefinite : it appears that the breakdown of laminar flow is caused by disturbances in the tunnel stream and that the effect of surface waviness is small.

(iv) The lowest value of C_{D_0} measured on the wooden model, $c = 70$ in., is 0·0032 at a Reynolds number 3·7 millions. This model has a more wavy surface than that of the metal-skin model, and the breakdown of laminar flow is due to the combined action of tunnel turbulence and surface waviness.

(v) The lowest value of C_{D_0} measured on the wooden model, $c = 42$ in., in the 9 ft. × 7 ft. tunnel is 0·0034 at a Reynolds number 2·6 millions : and this lower Reynolds number compared with that for the metal-skin model is due to the more wavy surface.

(vi) Tests on the wooden model, $c = 42$ in., and on spheres show that the flow in the 9 ft. × 7 ft. tunnel is steadier than that in the 13 ft. × 9 ft. tunnel.

(vii) The measured pressure distribution for infinite span agrees closely with the theoretical distribution, except at the tail, $x > 0{\cdot}95c$.

(viii) The flow at the median section of a model of aspect ratio 0·50 at 0 deg. incidence resembles that for infinite span, but the forward movement of transition and rise in C_{D_0} occur at a somewhat lower Reynolds number.

(ix) The positions of transition on all the wind-tunnel models, for Reynolds numbers below that for which C_{D_0} has its lowest value are near the calculated position of the laminar boundary-layer separation.

---

1. *Introduction.*—1.1. Aerodynamic characteristics of laminar-flow aerofoils must be measured at high Reynolds numbers and in a stream substantially free from turbulence if the results obtained are to be applicable to design. These conditions are common to flight but not to wind tunnels, except those of special design.

1.2. It was suggested some months ago[1] that the flow in the airstream of the National Physical Laboratory 13 ft. × 9 ft. tunnel, then under construction, would probably be sufficiently steady to allow the aerodynamic properties of laminar-flow aerofoils to be effectively studied up to a high Reynolds number, and, if this were found to be so, that measurements on laminar-flow aerofoils in this tunnel should be made as soon as possible, to supplement those obtained from flight researches. It was known, however, that it would be some months before the tunnel would be ready for service, and, in view of the urgency of the need for a fuller understanding of the behaviour of laminar-flow sections, it was further suggested that an interim test should be made in the William Froud National Tank at the N.P.L. It was realised that the success of the Tank experiment would depend on whether the disturbances created by the running of the model prevented the existence of a laminar boundary layer over a large part of the model surface, and that the results might be difficult to interpret, because of the restriction on aspect ratio which would arise from the large chord, needed to obtain a high Reynolds number, and from the limited depth of immersion. In spite of such uncertainties, approval for the test was given by the Aeronautical Research Council : for if the test were successful a valuable technique for the investigation of laminar-flow sections would be established because of the simplicity of drag measurement and of the ease and accuracy with which models can be cut in paraffin wax.

1.3. A scheme of test was considered with Dr. G. S. Baker, to whom the writers are indebted for advice and close co-operation. It was decided to measure by the pitot-traverse method the profile drag of laminar-flow aerofoil EQH 1260 at 0 deg. incidence. This aerofoil has a

symmetrical section and a maximum thickness $0{\cdot}12c$ at $0{\cdot}6c$. A model having a 10 ft. chord was made and the drag of the section 3 ft. below the still water surface was measured under Dr. Baker's supervision and with the help of L. T. G. Clarke of the Tank Department. The values of C_{D_0} measured were appreciably higher than those which would have been obtained if the boundary layer were laminar up to the point of minimum pressure : and to obtain information which would indicate whether the failure to measure a low drag was due to an earlier transition caused by water disturbances, or to a departure from two-dimensional flow, measurements of drag and pressure were made, in one of the 9 ft. $\times$ 7 ft. tunnels, for the median section of a model having the same aspect ratio as that of the Tank model, and also for the median section of a model spanning the tunnel from floor to roof. It appears that the failure to measure a low drag in the Tank experiment was partly due to the low aspect ratio, but more particularly to an early transition caused by water disturbances.

1.4. The 13 ft. $\times$ 9 ft. Tunnel came into service soon after the completion of these experiments, and the opportunity was taken to measure the drag of a large wooden model, $c = 70$ in., spanning this tunnel from floor to roof. The lowest value of C_{D_0}, $0{\cdot}0032$, occurred at a Reynolds number, $3{\cdot}7$ millions, which was lower than that expected. A model with a less wavy surface was then obtained by covering this wooden model with a thin metal sheet, and the lowest value of C_{D_0} obtained was $0{\cdot}0030$ at the appreciably higher Reynolds number $5{\cdot}4$ millions. The rise in C_{D_0} beyond this number was very steep and of the nature that would be expected from a breakdown of laminar flow in the boundary layer due to casual disturbances in the tunnel stream.

2. *Experiments in the William Froude National Tank.*—2.1. Aerofoil EQH 1260 is one of the ellipse-quartic-hyperbola series of laminar-flow aerofoils developed by Dr. Goldstein. Ordinates of this section are given in Table 1 and the shape of the section is given in Fig. 2. Table 2 gives the theoretical velocity and pressure distributions for two-dimensional flow calculated by Dr. Goldstein for 0 deg. incidence. The model was cut in paraffin wax. The chord was 10 ft. and the span $6{\cdot}5$ ft. The section was uniform along the span, except at the lower end where the edges were rounded. The model was mounted vertically on the Tank carriage, with a $5{\cdot}5$ ft. depth of immersion below the still water level. A horizontal shelf plate extending laterally 9 in. from the sides of the model, 18 in. forward from the leading edge and 36 in. behind the trailing edge, and a smaller bow shelf plate above the main shelf plate, were fitted on the model (*see* photograph, Fig. 1), to lessen wave formation. The main shelf plate was 6 in. below the still water level, and remained immersed at all speeds of test.

2.2. The drag of the section 3 ft. below the still water level, that is, midway between the main shelf plate and the lower end of the model, was measured by the pitot-traverse method. The comb used had eleven total-head tubes, external tube diameter $0{\cdot}114$ in. and average tube spacing $0{\cdot}381$ in. The tubes were carried by, and projected 6 in. in front of, a horizontal streamline strut, 14 in. long, attached at its ends by vertical streamline struts and tension wires to the Tank carriage. Static pressure was measured with two tubes carried on the horizontal strut, the holes of one tube being 3 in. above the mouth of the centre total-head tube, and those of the other the same height above the mouth of an end tube. The exploration plane was 1 ft. behind the trailing edge of the model. The datum pitot-static tube was immersed 3 ft. below the still water level, 5 ft. forward of the leading edge of the model and midway between the model and one wall of the tank. The tubes of the comb and the datum tubes were connected to the lower ends of the tubes of a manometer, the upper ends being connected to an airtight reservoir. The pressure within the reservoir was suitably adjusted before each run to ensure that the water levels were within the manometer scale. The positions of the water levels in the tubes were photographically recorded after the carriage had reached a constant speed and after the water in each tube had had time to respond fully to the pressure at its mouth. The velocities given by the datum pitot-static tube agreed within $\pm$ 1 per cent. with standard measurements of the carriage speed.

2.3. Profile drag was determined from the measurements of total head and static pressure by the relation, due to Professor Jones[2]

$$D = \tfrac{1}{2}\rho U_0^2 c \int_{\text{wake}} 2\left[g - \left(\frac{p - p_0}{\tfrac{1}{2}\rho U_0^2}\right)\right]^{1/2} [1 - g^{1/2}]\, d\left(\frac{y}{c}\right),$$

where D is the drag per unit span of the model at the section behind which the measurements were made, U_0 is the datum velocity,

$$g = \left[1 - \left(\frac{H_0 - H}{\tfrac{1}{2}\rho U_0^2}\right)\right],$$

H and p are the total head and pressure respectively in the wake, H_0 and p_0 are the datum total head and pressure respectively in the general stream and y is the distance across the wake. A correction to take account of the fact that the point in the mouth of a total-head tube at which the measured pressure acts is displaced from the geometric centre towards the side where the velocity is higher was added to values of the drag calculated, on the assumption that the pressure acted at the geometric centre. This correction on C_{D_0} is

$$+ 0{\cdot}72\frac{d}{c}\left[g - \left(\frac{p - p_0}{\tfrac{1}{2}\rho U_0^2}\right)\right]^{1/2} [1 - g^{1/2}],$$

where the values taken are those for the centre of the wake and d is the tube diameter.

Values of C_{D_0} obtained from the observations and those corrected for the effect of wall constraint (Appendix I) are given in Table 3. Curves of g, $(p - p_0)/\tfrac{1}{2}\rho U_0^2$ and

$$2\left[g - \left(\frac{p - p_0}{\tfrac{1}{2}\rho U_0^2}\right)\right]^{1/2} [1 - g^{1/2}]$$

plotted for $R = 4{\cdot}57 \times 10^6$, where $R = U_0 c/\nu$, are given in Fig. 3; the curves for $R = 6{\cdot}07 \times 10^6$ and $7{\cdot}66 \times 10^6$ show similar features, and for this reason are not included.

TABLE 3

Kinematic Viscosity (Water) $= 13{\cdot}25 \times 10^{-6}$ *ft.²/sec.*

U_0 ft./sec.	$R \times 10^{-6}$	C_{D_0} (measured)	C_{D_0} Corrected for wall constraint
6·06	4·57	0·0082	0·0081
8·03	6·07	0·0077	0·0076
10·15	7·66	0·0076	0·0075

The corrected values of C_{D_0}, plotted against R in Fig. 4, lie above the curve for a flat plate with a fully developed turbulent boundary layer extending over the whole of its length. The calculated positions of the transition points for the three speeds of test are about $0{\cdot}28c$ (Appendix II).

2.4. The failure to measure a low drag can be attributed to one or more of the following causes :—

(i) Roughness due to surface excrescences and/or surface waviness.

(ii) Model vibration.

(iii) A turbulent boundary-layer separation forward of the trailing edge.

(iv) Inherent turbulence and/or disturbances arising from surface wave and eddy formation.

(v) A departure from two-dimensional flow which favours an early transition.

The effect on drag of surface excrescences diminishes with their distance from the leading edge, and calculations made by the method outlined in " Modern Developments in Fluid Dynamics ", Chapter VII, pp. 316–319 (Ref. 3) show that excrescences on the forward part of the Tank model would have to project at least 0·004 in. from the surface to affect the drag. Excrescences of this size were not present. The surface appeared to be wavy when viewed by reflected light, but the depths of the hollows were minute compared with the distances between successive crests, so that the effect of waviness on the drag is likely to be small. The drag measurements were not affected by vibration, for the model ran smoothly through the water. There is no evidence to show whether the turbulent boundary layer at the tail separated from the surface forward of the trailing edge, but the results of the wind-tunnel experiments given later suggest that this did not occur. It would appear, therefore, that the high drag was due to water disturbances and/or a departure from two-dimensional flow which favours an early transition. It is shown later that the effect of the departure from two-dimensional flow is not likely to be important. The high drag measured on the Tank model arises in the main, therefore, from disturbances associated with wave and eddy formation. The change in these disturbances with speed, is such that the drag falls in the usual manner with an increase in Reynolds number (Fig. 4) : also, the effect of the disturbances on drag measurements for a given speed did not depend on the order in which the test runs were made nor on the time interval between them. Thus, the first run at 6·06 ft./sec. was made at the end of the first day of test, the second at the beginning of the second day (17 hours later), and the third and fourth runs after an interval during which several runs at a higher speed had been made : nevertheless, the results for the four runs are consistent with each other (Fig. 3).

3. *Experiments on Aerofoil EQH* 1260 *in the* 9 *ft.* × 7 *ft.* (*No.* 1) *and the* 13 *ft.* × 9 *ft. Wind Tunnels*.—3.1. The measurements made in the 9 ft. × 7 ft. Tunnel were the drag and the pressure distribution for

(i) the median section of a model having square ends and an aspect ratio 0·5,

(ii) the median section of a model having the edges of its end sections rounded and an aspect ratio 0·548,

(iii) the median section of a model spanning the tunnel from floor to roof, and

(iv) the pressure distributions for sections 0·214*c* from the median sections of models (i) and (ii).

Model (i) was made of wood, and had a hand-polished varnished surface. The chord was 42 in. The model was mounted vertically in the centre of the tunnel on two circular rods, attached to the tunnel floor and roof. The parts of the rods extending beyond the model were enclosed within streamline fairings (*see* Fig. 2). The alignment at 0 deg. incidence was made by angular adjustment until the pressures at corresponding holes in the two surfaces were equal.

Model (ii) was formed by model (i) with the attachment of end pieces 0·024*c* thick and rounded at the outer edges.

Model (iii), aerofoil spanning the tunnel from floor to roof, was formed by model (i) with extension pieces having the same section. Each extension piece was made in two halves, cut at the vertical plane of symmetry, so that they could be clamped on the vertical rods without disturbing the incidence setting of the middle part.

The models were hollow, to accommodate the pressure tubes. The experiments were made at 50, 100, 150 and 200 ft./sec. The corresponding values of R are 1·07, 2·13, 3·20 and 4·26 millions.

3.2. Profile drag was measured by the pitot-traverse method. The comb had 13 tubes, external tube diameter 0·068 in., spaced 0·20 in. apart, except the outer two at each end which were 0·50 in. apart. Measurements of static pressure were made with two tubes, one above the middle total-head tube and the other just outside the wake. The comb was mounted $0{\cdot}1c$ behind the trailing edge of a model. The total head and static pressure in the empty tunnel for the position of the mid-point of the median section were taken for datum values.

The measurements made in the 13 ft. × 9 ft. Tunnel were the drag for

(i) the median section of a wooden model spanning the tunnel from floor to roof, and

(ii) the same model with the middle 4 ft. span covered with a thin metal skin (aluminium).

The chord of the wooden model was 70 in. and that of the metal-skin model was 70·4 in. The total head and static pressure traverses were made for incidences from 0 to 4·5 deg., with the comb described above, but with the addition of four tubes, two on each side and spaced 0·5 in. apart. The traverses were made at $0{\cdot}1c$, except a few at $0{\cdot}013c$, behind the trailing edge.

3.3. *Pressure Measurements, Wooden Models, c = 42 in.*—The measured pressure coefficients $(p - p_0)/\frac{1}{2}\rho U_0^2$ were referred to a datum pressure, p_0, in the empty tunnel at the position of the mid-chord point of the median section. The pressure drop down the tunnel was small, $0{\cdot}0009\rho U_0^2$ per ft., and was not taken into account in the calculation of the pressure coefficients.

The pressure coefficients for a model were almost independent of wind speed, except near the tail : and the coefficients for the square-ended aerofoil, aspect ratio 0·5, were almost the same as those for the round-end aerofoil, aspect ratio 0·548. The results for the model spanning the tunnel, and taken for $R = 1{\cdot}07$ and 4·26 millions, and those for the round-end model, $R = 3.20$ millions, are plotted in Fig. 2. The theoretical pressure distribution for two-dimensional flow in an infinite stream, 0 deg. incidence, is given by the dotted curve. The full-line curve above the dotted curve is that for two-dimensional flow with tunnel-wall constraint, determined on the assumption that the effect for the model is the same as that for a Rankine oval having the same chord and maximum thickness. The effect of tunnel-wall constraint on a 12 per cent. thick Rankine oval in a tunnel whose breadth is $2{\cdot}57c$ (= breadth of tunnel/model chord) is to increase the theoretical surface velocity by 1·0 per cent. (R. & M. 1223[6], Table 1). For this increase in velocity

$$\left[\frac{p - p_0}{\frac{1}{2}\rho U_0^2}\right]_{\text{tunnel}} = 1{\cdot}02\left[\frac{p - p_0}{\frac{1}{2}\rho U_0^2}\right]_{\text{infinite stream}} - 0{\cdot}020\,.$$

Fig. 2 shows that the measured values of $(p - p_0)/\frac{1}{2}\rho U_0^2$ for the model spanning the tunnel fall closely on the theoretical curve for two-dimensional flow in the tunnel. The pressure coefficients for the median section of the model of aspect ratio 0·548 are about 0·065 greater than those for the model spanning the tunnel, and there is a general resemblance between the shapes of the curves drawn through the two sets of coefficients from $x = 0{\cdot}2c$ to $0{\cdot}75c$.

3.4. The theoretical pressure distribution for the median section of the aerofoil of aspect ratio 0·548 cannot be calculated, but an indication of the nature of the difference from that for infinite span can be obtained from a comparison of the minimum pressure on an ellipsoid with that on an elliptic cylinder of infinite span, whose section, normal to the span, is the same as that of the median section of the ellipsoid. It can be shown from relations given in Ref. 5 that the

maximum theoretical velocity on the surface of an ellipsoid is $1 \cdot 066U_0$, when the maximum thickness ($2c$) is $0 \cdot 12$ of the chord (2a), and the span (2b) is $0 \cdot 5$ of the chord. The maximum theoretical velocity for the elliptic clyinder is $1 \cdot 12U_0$. The corresponding values of the minimum pressure are $-0 \cdot 069\rho U_0^2$ and $-0 \cdot 128\rho U_0^2$, so that the minimum pressure on the ellipsoid is $0 \cdot 059\rho U_0^2$ greater than that on the elliptic cylinder. For an ellipsoid whose span is equal to the chord of the median section the minimum pressure is $0 \cdot 035\rho U_0^2$ greater. It is to be expected that the difference between the minimum pressure for the model of aspect ratio $0 \cdot 548$ and that of infinite span would be smaller than the difference between the minimum pressure for an ellipsoid whose span is $0 \cdot 548$ the chord of the median section and that for an elliptic cylinder of infinite span. Actually, the measured difference between the minimum pressures for the models, namely, $0 \cdot 033\rho U_0^2$, is very closely the same as the difference for an ellipsoid whose span is equal to the chord of the median section and an infinite elliptic cylinder.

Fig. 2 shows that the shape of the pressure curve for the section $0 \cdot 214c$ from the median section of the aerofoil of aspect ratio $0 \cdot 548$ differs from that for the median section. Instead of a continuous fall to the minimum pressure at $x = 0 \cdot 72c$, there is a rising pressure from $x = 0 \cdot 2c$ to $0 \cdot 42c$, followed by a falling pressure to a minimum at $x = 0 \cdot 74c$.

Drag Measurements.—3·5. The values of C_{D_0} measured for the models tested in the 9 ft. × 7 ft. Tunnel are given in Table 4, and those for the 13 ft. × 9 ft. Tunnel in Table 5. The values of C_{D_0} corrected for tunnel-wall constraint (*see* Appendix I) are given in the last columns of these Tables. These values are plotted against $\log_{10} R$ in Fig. 4, and in Fig. 8, where calculated curves of C_{D_0} against $\log_{10} R$ for fixed positions of the transition point (*see* Appendix II) are given.

(i) *Models of Aspect Ratio* $0 \cdot 5$ *and* $0 \cdot 548$.—3.6. The values of C_{D_0} measured for the median sections of the wind-tunnel models are practically the same. The lowest value of C_{D_0}, $0 \cdot 0042$, occurs at $R = 2 \cdot 1$ millions, whereas for infinite span ($c = 42$ in. and same tunnel) the lowest value is $0 \cdot 0034$ at a Reynolds number $2 \cdot 6$ millions. The values of C_{D_0} for the Tank model are much greater than those for the wind-tunnel models. At $R = 4 \cdot 2$ millions the value of C_{D_0} for the wind-tunnel models (aspect ratios $0 \cdot 5$ and $0 \cdot 548$) is $0 \cdot 0061$, whereas an extrapolated value for the Tank model is $0 \cdot 0080$. Further it would appear from the general trend of the curves in Fig. 4 that if a measurement for the Tank model had been made at $R = 2 \cdot 1$ millions, the value of C_{D_0} obtained would have been much greater than the value, $0 \cdot 0042$, measured for the wind-tunnel model of the same aspect ratio. The failure to measure a low drag in the Tank is due, therefore, partly to the low aspect ratio of the model, partly to the high Reynolds numbers at which the measurements were made, but more particularly to disturbances arising from eddy and wave formation caused by the motion of the model through the water.

The estimated position of the transition point on the wind-tunnel model, for the Reynolds number for which C_{D_0} has its lowest value, is $0 \cdot 80c$. The positions on the Tank model for the Reynolds numbers of experiment are about $0 \cdot 28c$. It should be added that the results of recent flight experiments show that drag measurements on laminar-flow panels of small span constructed on aeroplane wings may be less reliable than transition measurements as a guide to section characteristics : or in other words, that the drag calculated by the Squire-Young method for the measured pressure distribution may not be in agreement with the measured drag[4].

(ii) *Models of Infinite Span.*—3.7. The curves of C_{D_0} against $\log_{10} R$ for the models of infinite span exhibit the same general characteristic : a fall of C_{D_0} to a minimum value followed by a rise with increasing Reynolds number (Fig. 4). The minimum value of C_{D_0}, the Reynolds number at which it occurs, and the nature of the rise in C_{D_0} beyond this Reynolds number depend on surface roughness, surface waviness and the turbulence in the tunnel stream. It is improbable that surface roughness of the models has a measurable effect on C_{D_0} at the Reynolds numbers of the experiments.

3.8. *Wooden Model, $c = 70$ in., and Metal-Skin Model. $c = 70{\cdot}4$ in., 13 ft. $\times$ 9 ft. Tunnel.*— Wooden model, $c = 70$ in., was the first to be tested in the 13 ft. $\times$ 9 ft. Tunnel. The lowest value of C_{D_0} did not occur at as high a Reynolds number as that expected, and to find out to what extent this shortcoming was due to surface waviness measurements of C_{D_0} were made on this model after it had been covered with a metal skin. The skin was formed of aluminium sheet which was attached to the model at the Royal Aircraft Establishment by the method used for laminar-flow wings. The improvement in surface waviness due to the metal skin is shown by a comparison of the full-line curves in Fig. 10, which are drawn through readings taken with a curvature gauge. The two feet of the gauge were 3 in. apart, and the readings, taken with an Ames dial, gave a height of a pointer midway between and above a base line located by the feet. The readings plotted were taken every $0{\cdot}5$ in. The dotted curve of each diagram gives the reading calculated for a model with a non-wavy surface. The full-line curves do not, of course, give a true measure of the waviness of a surface, but they do show that the waviness of the surface of the model with the metal skin is appreciably less than that for the wooden model: thus, the readings for the metal-skin surface lie within $\pm 0{\cdot}002$ in. from the dotted curve, whereas those for the wooden surface are only within $\pm 0{\cdot}007$ in. The waviness of the metal-skin surface compares favourably with metal surfaces of wings found to be satisfactory in flight at Reynolds numbers above those of the present experiments. It should be stated that subsequent investigation leads to the conclusion that wooden models can be made with surfaces appreciably less wavy than that shown in Fig. 10. It was found that the waviness of the surface of a wooden model followed closely that of its template, and that improvement in the template, obtained by rubbing down the peaks, resulted in a corresponding improvement in the waviness of the surface of the model. Unfortunately, it appears probable that the surface waviness of a wooden model changes with time.

3.9. The improvement in surface waviness arising from the attachment of the metal skin results in a fall in the lowest value of C_{D_0} from $0{\cdot}0032$ to $0{\cdot}0030$, and, more important, an increase in the Reynolds number at which the lowest value of C_{D_0} occurs from $3{\cdot}7$ millions to $5{\cdot}4$ millions (Fig. 4). The rise in C_{D_0} beyond this Reynolds number is much steeper for the metal-skin model than for the wooden model: and the measurements of C_{D_0} beyond the lowest value are more indefinite for the metal-skin model. Thus, at $\log_{10} R = 6{\cdot}79$, the flow remained sufficiently steady to allow the low value $C_{D_0} = 0{\cdot}00287$ (*see* Fig. 4) to be measured: but occasionally, without any change in tunnel speed, the wake shifted sideways, a probable indication of an earlier breakdown of flow in the boundary layer on one surface than on the other, and the drag increased greatly. On one occasion, the wake did not shift sideways, but it appeared from a snap judgment made from the changes of levels in the manometer tubes that the drag had increased to about twice its low value. The general impression was that the breakdown of laminar flow in the boundary layer, and the increase in drag which accompanied this breakdown, arose from instability due to casual disturbances in the tunnel stream, and it is probable that the surface waviness was too small to matter. On the other hand, it is likely that the slow and steadier rise in C_{D_0} on the wooden model is due to the combined action of surface waviness and tunnel disturbances.

The estimated positions of the transition points on both models for the Reynolds numbers for which C_{D_0} is a minimum are about $0{\cdot}82c$ (Fig. 8). This position is close to the position of laminar-boundary layer separation, $0{\cdot}78c$, calculated by Falkner's method (Ref. 8).

3.10. Curves of C_{D_0} for the wooden aerofoil, $c = 70$ in., plotted against angle of incidence, for Reynolds numbers at and below the value for which C_{D_0} is a minimum, are given in Fig. 9. The value of C_{D_0} increases with incidence at first slowly but then rapidly. At 3 deg. the value of C_{D_0} is about double that at 0 deg., and about the same as that for the symmetrical section NACA 0012, whose maximum thickness, $0{\cdot}12c$, is at $0{\cdot}3c$. The mean position of the transition points on the two surfaces estimated for $R = 3{\cdot}79$ millions moves forward from $0{\cdot}82c$ at 0 deg. to $0{\cdot}62c$ at 2 deg. and $0{\cdot}21c$ at 4 deg.

3.11. *Wooden Model, $c = 42$ in., in the 13 ft. $\times$ 9 ft. and the 9 ft. $\times$ 7 ft. Tunnels.*—The lowest value of C_{D_0} for the wooden model $c = 42$ in., in the 13 ft. $\times$ 9 ft. Tunnel is 0·0041 and occurs at a Reynolds number 2·2 millions, whilst the lowest value for the same model in the 9 ft. $\times$ 7 ft. Tunnel is 0·0034 and occurs later at 2·6 millions (Fig. 4). The rise in C_{D_0} beyond its minimum value is due to the combined effect of disturbances in the tunnel stream and surface waviness on the flow in the boundary layer, and the earlier the rise the greater is this effect. It appears therefore that the flow in the 13 ft. $\times$ 9 ft. Tunnel is not so steady as that in the 9 ft. $\times$ 7 ft. Tunnel. Tests on spheres lead to the same conclusion. The critical number for a 6 in. sphere, determined from pressure measurements just behind the sphere[12], was 355,000 in the 13 ft. $\times$ 9 ft. Tunnel and 362,000 in the 9 ft. $\times$ 7 ft. Tunnel. The numbers for a 3 in. sphere in the 13 ft. $\times$ 9 ft. Tunnel were 334,000 (rising wind speed) and 326,000 (falling wind speed). Both these numbers are lower than that for the 6 in. sphere in the same tunnel, so that the fractional turbulence in the tunnel is greater at high speeds than at low speeds, for if the turbulence were independent of speed the critical number for the 3 in. sphere should be greater than that for the 6 in. sphere. The critical speed for a 3 in. sphere in the 9 ft. $\times$ 7 ft. Tunnel was beyond the highest speed of the tunnel, but the trend of the pressure measurements taken indicated that the critical number would be higher than that for the 6 in. sphere. It is likely therefore that the fractional turbulence in this tunnel is independent of the wind speed. A detailed exploration of the flow in the 13 ft. $\times$ 9 ft. Tunnel has not yet been made : and the reason for the increase in turbulence at the higher speeds is not known. It may be that larger and more persistent disturbances are shed at the higher speeds from the cascade of guide vanes in front of the honeycomb : but whether this is so or not, an attempt to improve the steadiness of flow at the higher speeds appears to be worth while.

3.12. *Wooden Models, $c = 70$ in. and $c = 42$ in., in the 13 ft. $\times$ 9 ft. Tunnel.*—The lowest value of C_{D_0} measured on the model, $c = 70$ in., is 0·0032 and occurs at a Reynolds number 3·7 millions, whereas the lowest value of C_{D_0} measured on the model, $c = 42$ in., is 0·0041 at a Reynolds number 2·3 millions (Fig. 4). The curves of rising C_{D_0} correspond in shape. The tunnel speeds at which C_{D_0} is a minimum are about the same (105 ft./sec.) for the two models, so that the disturbances in the stream are the same, and, apart from the effect of surface waviness, it is to be expected that the lowest value of C_{D_0} would occur at a higher Reynolds number for model, $c = 42$ in., than that for the larger model, $c = 70$ in. It appears from measurements taken with the curvature gauge, however, that the surface of model, $c = 42$ in., is more wavy than that of model, $c = 70$ in., and this probably accounts for the earlier rise in C_{D_0} for model, $c = 42$ in.

3.13. The dotted curves of Fig. 4 give the change in C_{D_0} or $C_{D_{0\min.}}$ as the case may be, with $\log_{10} R$ for aerofoil NACA 0012, Piercy aerofoil 1240, aerofoil EQ 1250/1050 and aerofoil NACA 18–212. The tests on the first three aerofoils were made in the Compressed-air Tunnel and that on NACA 18–212 in the N.A.C.A. Two-dimensional Flow Tunnel. The maximum thickness of each of these aerofoils is 0·12 of the chord, and, in the order given, is 0·3, 0·4, 0·5 and 0·6 of the chord from the leading edge. These curves, together with those for the EQH 1260 models, show the fall in the lowest value of C_{D_0} (or $C_{D_{0\min.}}$) and the increase in the value of the Reynolds number at which the lowest value occurs with the distance of the position of the maximum thickness from the leading edge : but a strict comparison is not possible because the conditions of test are different. Aerofoil NACA 18–212 has an unsymmetrical section designed to have minimum drag at $C_L = 0·2$, and it will be noticed that the lowest value of $C_{D_{0\min.}}$ is 0·0033 at a Reynolds number 5 millions. These figures do not differ much from those, 0·0030 at 5·5 millions, for the metal-skin model in the 13 ft. $\times$ 9 ft. Tunnel. There is, in addition, a close resemblance in the nature of the rise in C_{D_0} (or $C_{D_{0\min.}}$) beyond the lowest value. The flow in the 13 ft. $\times$ 9 ft. Tunnel is, therefore, not greatly different from that in the N.A.C.A. Two-dimensional Flow Tunnel, assuming, of course, that there is no important difference in the surface waviness of the models.

4. *Conclusions.*—The main conclusions which can be drawn from the paper are as follows :—

(i) The flow conditions in the 13 ft. × 9 ft. and the 9 ft. × 7 ft. Tunnels are sufficiently steady to allow the properties of laminar-flow aerofoils to be investigated up to a Reynolds number, U_0C/ν, about 5 millions.

(ii) The William Froude National Tank cannot be used to investigate the properties of laminar-flow aerofoils at high Reynolds numbers, unless an experimental technique can be devised for which disturbances due to surface wave and eddy formation do not matter.

(iii) The best surface was obtained on a model covered with thin metal sheet for which the readings given by a curvature gauge, whose feet were 3 in. apart, agreed with the calculated values within $\pm$ 0·002 in. For this model the Reynolds number at which the rise in C_{D_0} associated with the forward movement of transition occurs appears to be fixed by disturbances in the tunnel stream.

(iv) The positions of transition on all the wind-tunnel models, for Reynolds numbers below that for which C_{D_0} has its lowest value, are near the calculated position of laminar boundary-layer separation.

(v) The flow at the median section of a model of aspect ratio 0·50 at 0 incidence resembles that for infinite span : but the lowest value of C_{D_0} is greater and the Reynolds number at which it occurs is lower.

5. *Acknowledgment.*—The experiments in the 13 ft. × 9 ft. Tunnel were made with the assistance of R. J. Cox.

REFERENCES

No.	*Author*	*Title, etc.*
1	A. Fage	Laminar-flow Wing Sections. A.R.C. 4552. 1940. (Unpublished.)
2	The Cambridge University Aeronautics Laboratory	The Measurement of Profile Drag by the Pitot-traverse Method. R. & M. 1688. 1936.
3	Edited by S. Goldstein	Modern Developments in Fluid Dynamics. The Clarendon Press, Oxford. 1938.
4	G. E. Pringle, H. B. Squire and K. J. Lush	Interim Note on Flight Tests of Low-drag Sections at the Royal Aircraft Establishment. A.R.C. 4521. 1940. (Unpublished.)
5	W. F. Durand, Editor-in-Chief	Aerodynamic Theory. Julius Springer. Berlin. 1934. Vol. I, Division C, Chapter VIII.
6	A. Fage	On the Two-dimensional Flow Past a Body of Symmetrical Cross-section in a Channel of Finite Breadth. R. & M. 1223. 1929.
7	D. H. Williams and A. F. Brown ..	Tests on Aerofoil EQ 1250/1050 with and without Flap, in the C.A.T. A.R.C. 5517. 1941. (To be published.)
8	V. M. Falkner	Simplified Calculation of the Laminar Boundary Layer. R. & M. 1895. July, 1941.
9	A. D. Young and N. E. Winterbottom ..	Note on the Effect of Compressibility on the Profile Drag of Aerofoils at Subsonic Mach Numbers in the Absence of Shock Waves. R. & M. 2400. May, 1940.
10	H. B. Squire and A. D. Young	The Calculation of the Profile Drag of Aerofoils. R. & M. 1838. 1937.
11	N. E. Winterbottom and H. B. Squire ..	Note on Further Wing Profile Drag Calculations. (Addendum to R. & M. 1838.) A.R.C. 4871. 1940.
12	A. Fage	Experiments on a Sphere at Critical Reynolds Numbers. R. & M. 1766. 1937.
13	E. N. Jacobs	Preliminary Report on Laminar-flow Aerofoils and New Methods adopted for Aerofoil and Boundary-layer Investigations. N.A.C.A. Wartime Report No. L-345. May, 1947. A.R.C. 5427.
14	R. Jones and D. H. Williams	Effect of Surface Roughness on Characteristics ofAerofoils NACA 0012 and RAF 34. R. & M. 1708. 1936.

APPENDIX I

Effect of Tunnel-Wall Constraint

Tunnel-wall constraint increases the velocity at the surface of a model. When the flow in the boundary is laminar over the entire surface the drag is proportional to (local velocity)$^{1\cdot5}$, and when it is turbulent over the entire surface the drag is closely proportional to (local velocity)$^{1\cdot8}$. The drag of a model in a tunnel therefore lies between $(1 + m)^{1\cdot5}$ and $(1 + m)^{1\cdot8}$, that is, between $(1 + 1\cdot5m)$ and $(1 + 1\cdot8m)$ times the drag in an infinite stream, where $(1 + m)$ is the ratio of the surface velocity in the tunnel to that in an infinite stream. The value of the drag for a model in an infinite stream can therefore be taken to be $(1 - 1\cdot65m)$ times the drag in the tunnel, since m is small. The value of m for a model was obtained on the assumption that it is the same as the theoretical value for a Rankine oval having the same chord and maximum thickness. Values of m calculated for wide ranges of c/T and H/T, where c = chord, T = maximum thickness and H = tunnel breadth, are given in Ref. 6. The value of m for the models in the 9 ft. × 7 ft. Tunnel is 0·010, that for the large models in the 13 ft. × 9 ft. Tunnel is 0·012, and that for the model in the Tank is 0·009.

APPENDIX II

Calculation of Profile Drag

To allow estimations of the position of transition point to be made, curves of C_{D_0} against $\log_{10} R$ were calculated for selected positions of the transition point by the method of Squire and Young[10]. The measured distribution of velocity, u_1/U_0, given in Fig. 5, was taken, and afterwards curves of C_{D_0} against $\log_{10} R$ for an infinite stream were obtained in the manner described in Appendix I. The calculations for the laminar boundary layer were made by Falkner's method[8], and by the simplified Kármán-Pohlhausen method due to Young and Winterbottom[9]. The values of the momentum thickness, θ, obtained by the two methods for the front part of the section up to the point of maximum surface velocity were in close agreement (± 1 per cent.) : but the values of skin-friction intensity, $\tau_0/\frac{1}{2}\rho U_0^2$, differed by amounts lying within ± 5 per cent. Beyond the point of maximum surface velocity, Falkner's method, which is the more reliable, was used. The calculations for that part of the surface over which the flow in the boundary layer is turbulent were made by the method described in R. & M. 1838[10].

Curves showing the distributions of $\tau_0/\frac{1}{2}\rho U_0^2$ over the entire surface for $R = 3\cdot16 \times 10^6$ and $R = 10^7$ are given in Fig. 5. The curves for $R = 10^6$ are not included, but they show the same features. The values of C_{D_0} obtained from the calculations are given in Table 6.

TABLE 6

Values of C_{D_0}

	Position of transition point x/c	$R = 10^6$	$R = 3\cdot162 \times 10^6$	$R = 10^7$
Calculated for the measured u_1/U_0 curve of Fig. 5	0·24	0·01161	0·00912	0·00732
	0·49	0·00934	0·00701	0·00551
	0·74	0·00652	0·00451	0·00331
Values for infinite stream ..	0·24	0·01142	0·00897	0·00720
	0·49	0·00919	0·00689	0·00542
	0·74	0·00641	0·00444	0·00326

To obtain an indication of the dependence of C_{D_0} on the shape of the u_1/U_0 curve at the tail, calculations were made for the curve modified in the manner shown by the dotted line of Fig. 5 : the values of C_{D_0} obtained were about 1 per cent. greater.

The curves of Fig. 7 show the change in the calculated value of C_{D_0} with the distance of the maximum thickness ($0{\cdot}12c$) from the leading edge, for fixed positions of the transition point. The values of C_{D_0} for maximum thickness at $0{\cdot}3$ chord were taken from R. & M. 1838[10], and those for $0{\cdot}5$ chord from Ref. 11. The value of C_{D_0} increases linearly with the distance of the maximum thickness from the leading edge. The increase for a change in position from $0{\cdot}3c$ to $0{\cdot}6c$ and a fixed position of transition point lying between $0{\cdot}24c$ and $0{\cdot}74c$ is $0{\cdot}0010$. The measured values of u_1/U_0 for the median sections of the models of aspect ratio $0{\cdot}5$ and $0{\cdot}548$ are about $0{\cdot}984$ of those for infinite span and the same datum velocity. The ratios of the calculated values of C_{D_0} for these sections to those for infinite span would therefore lie between $(0{\cdot}984)^{1{\cdot}5}$, *i.e.*, $0{\cdot}976$, the ratio for a laminar boundary layer over the entire surface, and $(0{\cdot}984)^{1{\cdot}8}$, *i.e.*, $0{\cdot}971$, the ratio for a turbulent boundary layer over the entire surface. These two values are so close that the mean value $0{\cdot}974$ can be taken for all positions of the transition point. The positions of the transition point for these sections can therefore be determined from the measured value of C_{D_0}, corrected for wind-tunnel constraint, and the calculated curves of Fig. 8, if the scale of C_{D_0} is multiplied by $0{\cdot}974$, or alternatively from the curves without a change of scale for values of C_{D_0} $1/0{\cdot}974$ greater. The values of C_{D_0} for the model of aspect ratio $0{\cdot}548$, corrected for tunnel-wall constraint are plotted (points in circles) : and the curve drawn parallel to and above the measured curve, obtained from the values of C_{D_0} multiplied by $1/0{\cdot}974$, is shown dotted.

TABLE 1

Aerofoil EQH 1260

Shape of section is given by

$$\left(\frac{y}{c}\right)^2 = 0{\cdot}012\frac{x}{c}\left(1 - \frac{5}{6}\frac{x}{c}\right),$$

$$i.e.\ \pm\frac{y}{c} = 0{\cdot}109545\sqrt{\frac{x}{c}\left(1 - \frac{5}{6}\frac{x}{c}\right)}$$

for $0 \leqslant x/c \leqslant 0{\cdot}6$,

$$\pm\frac{y}{c} = 0{\cdot}06 - 0{\cdot}083\dot{}\left(\frac{x}{c} - 0{\cdot}6\right)^2 - 1{\cdot}42527\dot{}\left(\frac{x}{c} - 0{\cdot}6\right)^3 + 1{\cdot}7871527\dot{}\left(\frac{x}{c} - 0{\cdot}6\right)^4$$

for $0{\cdot}6 \leqslant x/c \leqslant 0{\cdot}9760155$ and

$$\pm\frac{y}{c} = 0{\cdot}282147\sqrt{\frac{x_2}{c}\left(\frac{x_2}{c} + 0{\cdot}0109775\right)}$$

for $0{\cdot}9760155 \leqslant x/c \leqslant 1$, where x is the distance from the leading edge, $x_2 = (1 - x)$, and y is the ordinate.

Ordinates of Section

x/c	y/c	x/c	y/c	x/c	y/c
0	0	0·14	0·038523	0·72	0·056708
0·002	0·004895	0·18	0·042849	0·74	0·055142
0·004	0·006917	0·22	0·046433	0·76	0·053200
0·006	0·008464	0·26	0·049137	0·78	0·050864
0·008	0·009765	0·30	0·051962	0·80	0·048124
0·010	0·010909	0·34	0·054074	0·82	0·044977
0·014	0·012886	0·38	0·055821	0·84	0·041426
0·018	0·014586	0·42	0·057236	0·86	0·037483
0·025	0·017139	0·46	0·058344	0·88	0·033164
0·030	0·018735	0·50	0·059161	0·90	0·028493
0·035	0·020193	0·54	0·059699	0·92	0·023503
0·04	0·021541	0·58	0·059967	0·94	0·018230
0·05	0·023979	0·60	0·060000	0·96	0·012720
0·06	0·026153	0·62	0·059956	0·98	0·007023
0·08	0·029933	0·66	0·059415	0·99	0·004087
0·10	0·033166	0·70	0·057920	1	0

TABLE 2

Aerofoil EQH 1260

Theoretical Velocity and Pressure Distributions for Two-dimensional Flow

q = surface velocity, U_0 = stream velocity, x = distance along the chord and s = distance along the surface, measured from the forward stagnation point.

x/c	s/c	q/U_0	$\left(\frac{p-p_0}{2\rho U_0^2}\right)$
0	0	0	1·0000
0·0062	0·0111	0·9092	0·1734
0·0245	0·0313	1·0469	−0·0960
0·0546	0·0625	1·0804	−0·1673
0·0957	0·1042	1·0928	−0·1942
0·1468	0·1559	1·0995	−0·2089
0·2066	0·2160	1·1032	−0·2171
0·2737	0·2833	1·1066	−0·2246
0·3464	0·3561	1·1092	−0·2303
0·4229	0·4327	1·1131	−0·2390
0·5014	0·5112	1·1177	−0·2493
0·5799	0·5897	1·1307	−0·2785
0·6566	0·6665	1·1546	−0·3331
0·7295	0·7395	1·1677	−0·3635
0·7965	0·8069	1·1456	−0·3124
0·8559	0·8671	1·0923	−0·1931
0·9063	0·9187	1·0211	−0·0426
0·9466	0·9604	0·9409	+0·1147
0·9761	0·9909	0·8565	0·2664
0·9940	1·0095	0·7368	0·4571
1	1·0157	0	1·0000

TABLE 4

EQH 1260 *Models in* 9 *ft.* × 7 *ft. Tunnel*

c = 42 in. 0 deg. Incidence

	U_0 ft./sec.	$R \times 10^{-6}$	C_{D_0} Tunnel	C_{D_0} Corrected for tunnel-wall constraint
Model of infinite span	200	4·26	0·00536	0·00527
	150	3·20	0·00377	0·00371
	100	2·13	0·00367	0·00361
	50	1·07	0·00582	0·00573
Median section of model, aspect ratio 0·548	200	4·26	0·00610	0·00599
	150	3·20	0·00578	0·00569
	100	2·13	0·00426	0·00419
	50	1·07	0·00651	0·00640
Median section of model, aspect ratio 0·5	200	4·26	0·00617	0·00606
	150	3·20	0·00576	0·00567
	100	2·13	0·00429	0·00422
	50	1·07	0·00633	0·00622

TABLE 5

EQH 1260 *Models in the* 13 *ft.* × 9 *ft. Tunnel*

Infinite Span

		U_0 ft./sec.	$R \times 10^{-6}$	C_{D_0} Tunnel	C_{D_0} Corrected for tunnel-wall constraint
Metal-Skin Model—		48·9	1·93	0·00464	0·00455
$c = 70{\cdot}4$ in.		58·7	2·31	0·00432	0·00423
0 deg. Incidence.		68·5	2·69	0·00378	0·00371
Comb $0{\cdot}1c$ behind trailing edge.		78·4	3·08	0·00353	0·00346
		88·0	3·46	0·00337	0·00329
		97·8	3·85	0·00332	0·00326
		107·8	4·23	0·00314	0·00308
		127·2	5·01	0·00308	0·00302
		137·2	5·39	0·00292	0·00286
		137·2	5·39	0·00308	0·00302
		137·2	5·39	0·00391	0·00383
		156·8	6·16	0·00293	0·00287
		176·5	6·92	0·00655	0·00643
		176·5	6·92	0·00722	0·00708
Wooden Model—		74·8	2·76	0·00374	0·00367
$c = 70$ in.		99·5	3·67	0·00331	0·00325
0 deg. Incidence.		140·0	5·08	0·00442	0·00431
Comb $0{\cdot}1c$ behind trailing edge.		149·3	5·52	0·00525	0·00515
		180·0	6·56	0·00619	0·00607
		199·5	7·30	0·00650	0·00637
		231·0	8·20	0·00751	0·00736
Comb $0{\cdot}013c$ behind trailing edge.		49·2	1·89	0·00437	0·00428
		73·8	2·83	0·00330	0·00353
		98·3	3·77	0·00331	0·00325
Wooden Model—		78·6	1·77	0·00459	0·00458
$c = 42$ in.		108·3	2·43	0·00468	0·00466
Comb $0{\cdot}1c$ behind trailing edge.		138·0	3·09	0·00497	0·00496
		167·5	3·75	0·00570	0·00569
		197·0	4·42	0·00612	0·00611
		207·0	4·63	0·00724	0·00723
		226·5	5·08	0·00757	0·00756
Wooden Model—	0·5	74·0	2·84	0·00377	0·00370
$c = 70$ in.	0·5	98·6	3·79	0·00340	0·00333
Comb $0{\cdot}1c$ behind trailing edge.	1·0	74·0	2·84	0·00377	0·00370
Incidence, degrees, given in first column.	1·0	98·6	3·79	0·00430	0·00421
	1·5	49·3	1·90	0·00482	0·00472
	1·5	74·0	2·84	0·00431	0·00422
	1·5	98·6	3·79	0·00518	0·00508
	3·0	49·3	1·90	0·00771	0·00756
	3·0	74·0	2·84	0·00709	0·00695
	3·0	98·6	3·79	0·00709	0·00694
	4·5	49·3	1·90	0·01002	0·00982
	4·5	74·0	2·84	0·00913	0·00895

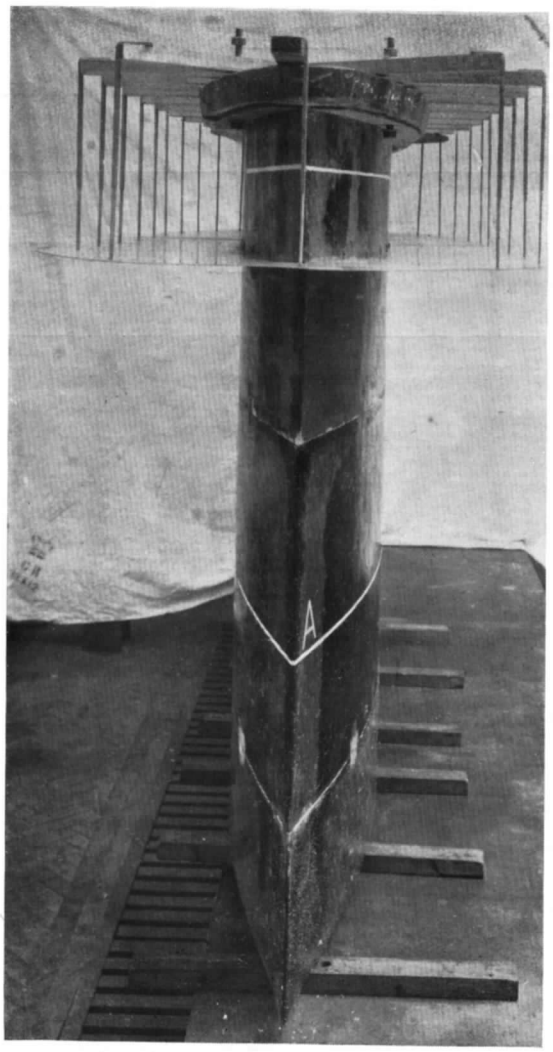

FIG. 1.

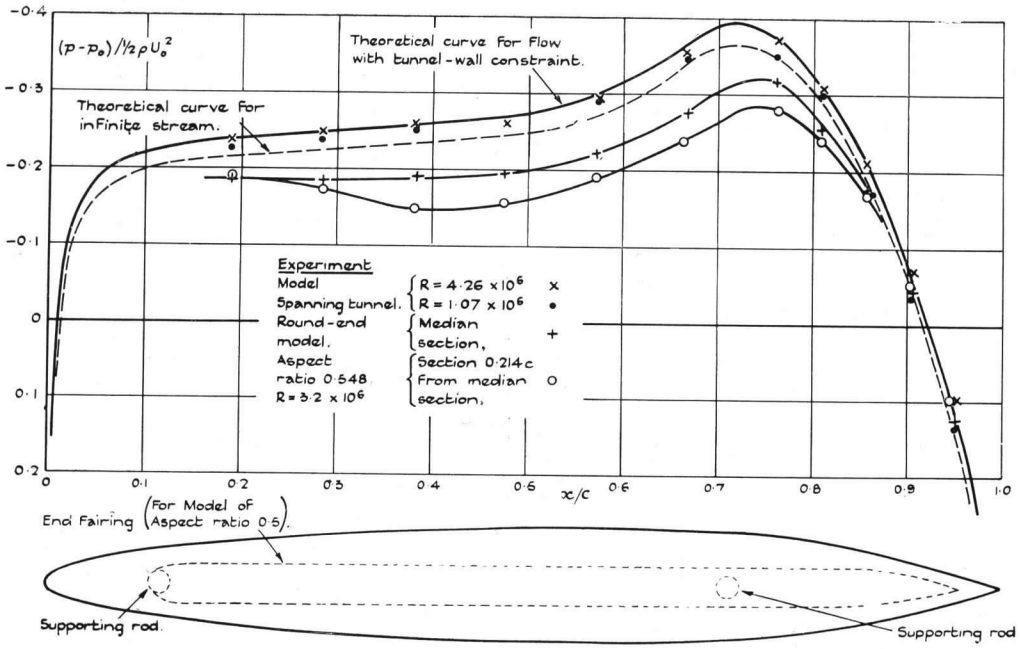

FIG. 2 Aerofoil EQH 1260. 0 deg. Incidence.

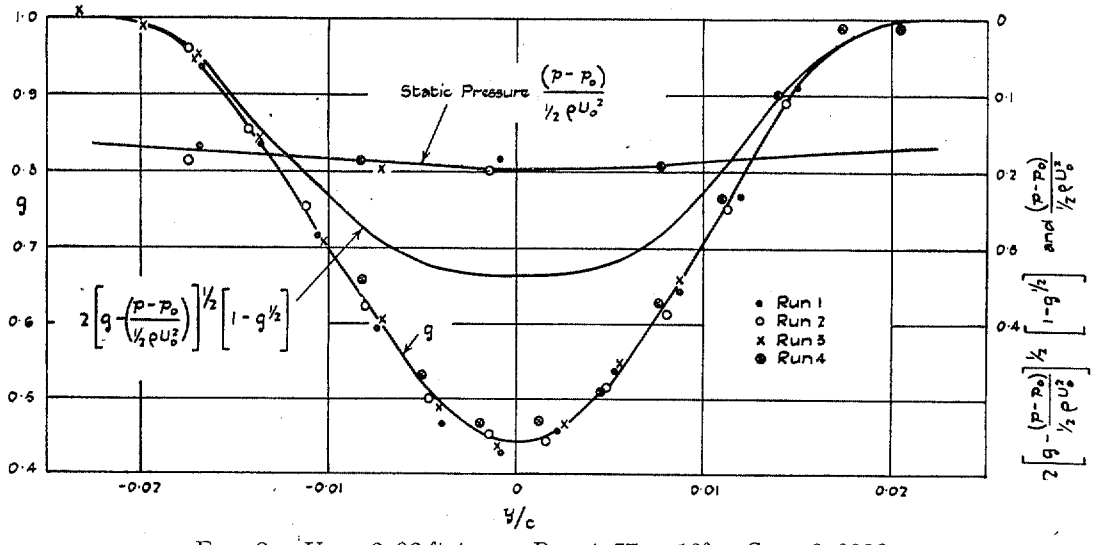

FIG. 3. $U_0 = 6{\cdot}06$ ft./sec. $R = 4{\cdot}57 \times 10^6$. $C_D = 0{\cdot}0082$.

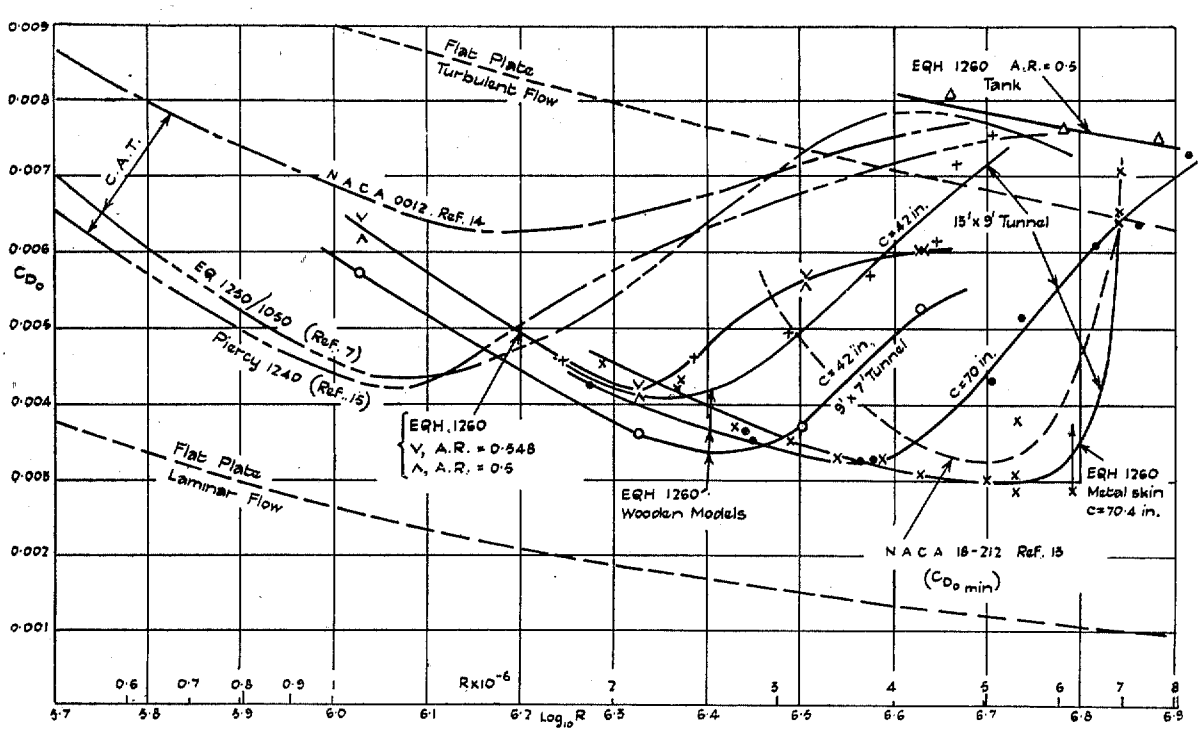

FIG. 4.

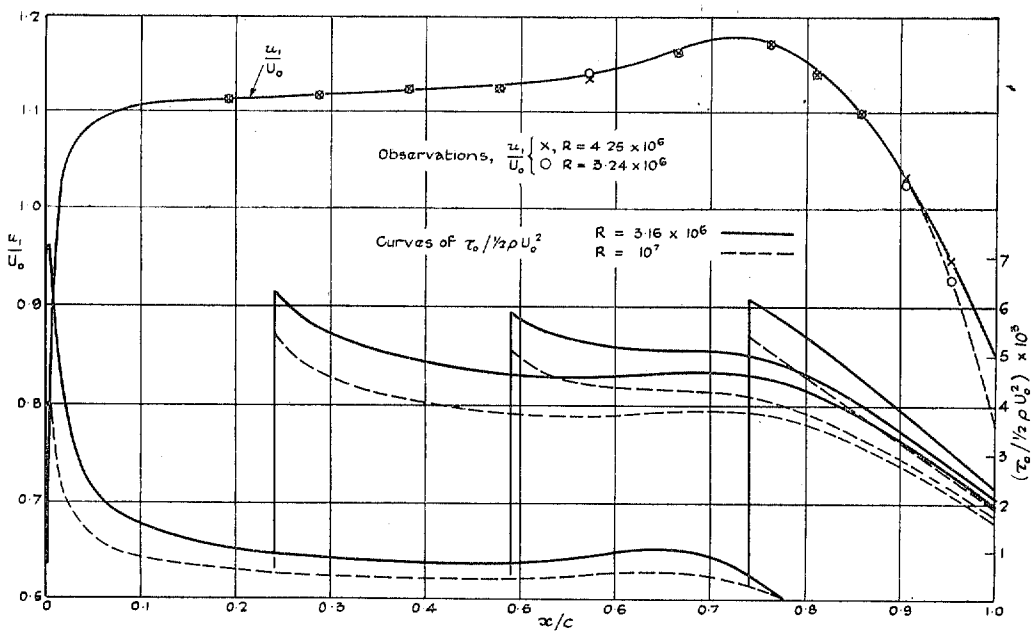

FIG. 5.

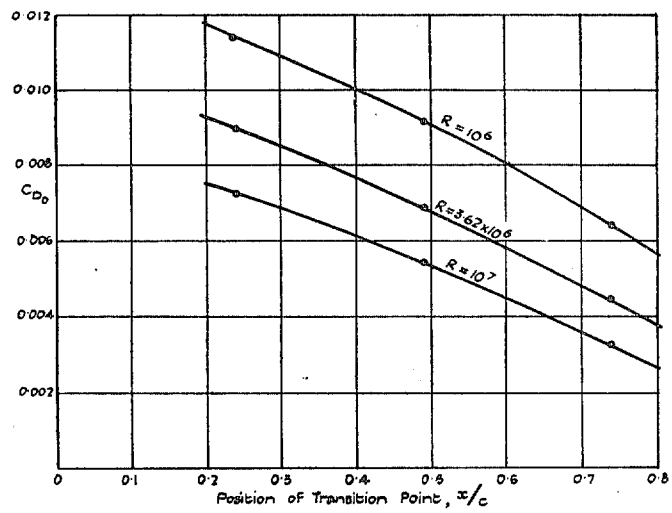

FIG. 6. Aerofoil EQH 1260.
Infinite Span. Incidence = 0 deg.

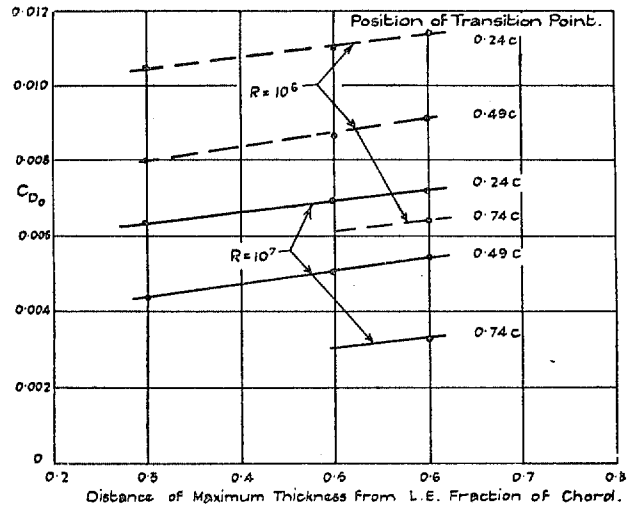

FIG. 7. Thickness = 0·12 Chord.

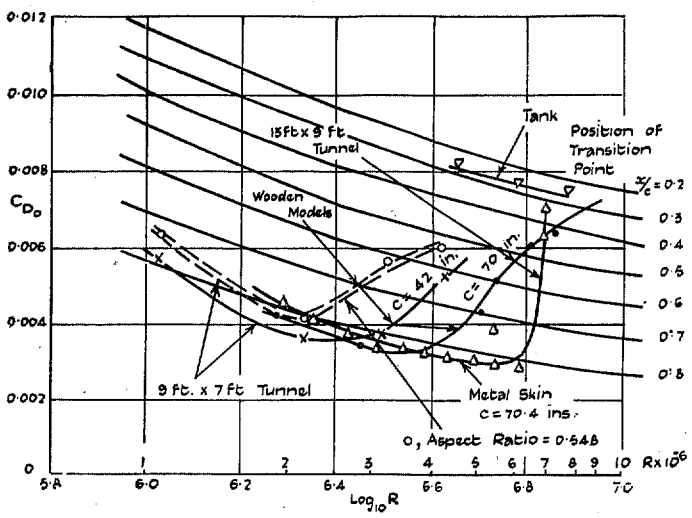

FIG. 8.

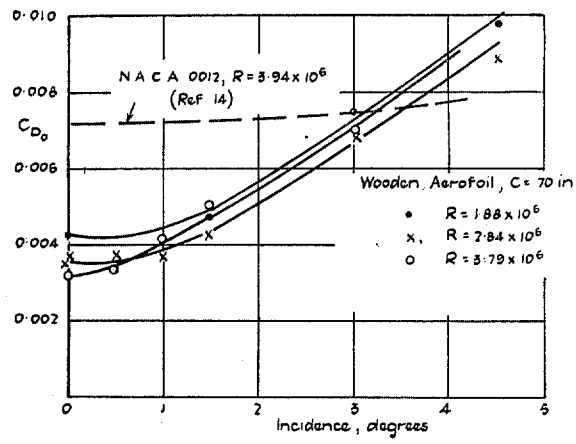

FIG. 9.

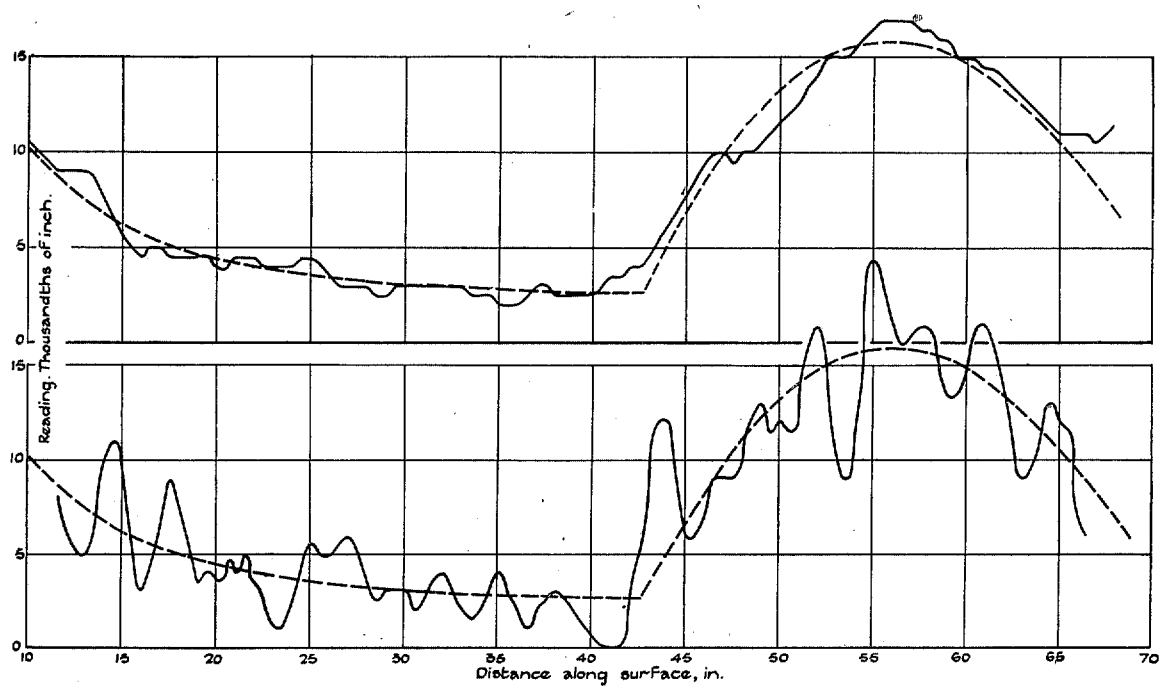

FIG. 10 (Upper Figure). Model with Metal Skin $c = 70{\cdot}4$ in.
(Lower Figure). Wooden Model $c = 70$ in.

85222) Wt. 12/818 12/48 Hw.

Publications of the Aeronautical Research Committee

TECHNICAL REPORTS OF THE AERONAUTICAL RESEARCH COMMITTEE—

1934-35 Vol. I. Aerodynamics. 40*s.* (40*s.* 8*d.*)
Vol. II. Seaplanes, Structures, Engines, Materials, etc. 40*s.* (40*s.* 8*d.*)

1935-36 Vol. I. Aerodynamics. 30*s.* (30*s.* 7*d.*)
Vol. II. Structures, Flutter, Engines, Seaplanes, etc. 30*s.* (30*s.* 7*d.*)

1936 Vol. I. Aerodynamics General, Performance, Airscrews, Flutter and Spinning. 40*s.* (40*s.* 9*d.*)
Vol. II. Stability and Control, Structures, Seaplanes, Engines, etc. 50*s.* (50*s.* 10*d.*)

1937 Vol. I. Aerodynamics General, Performance, Airscrews, Flutter and Spinning. 40*s.* (40*s.* 9*d.*)
Vol. II. Stability and Control, Structures, Seaplanes, Engines, etc. 60*s.* (61*s.*)

ANNUAL REPORTS OF THE AERONAUTICAL RESEARCH COMMITTEE—

1933-34 1*s.* 6*d.* (1*s.* 8*d.*)
1934-35 1*s.* 6*d.* (1*s.* 8*d.*)
April 1, 1935 to December 31, 1936. 4*s.* (4*s.* 4*d.*)
1937 2*s.* (2*s.* 2*d.*)
1938 1*s.* 6*d.* (1*s.* 8*d.*)

INDEXES TO THE TECHNICAL REPORTS OF THE ADVISORY COMMITTEE ON AERONAUTICS—

December 1, 1936 — June 30, 1939
Reports & Memoranda No. 1850. 1*s.* 3*d.* (1*s.* 5*d.*)

July 1, 1939 — June 30, 1945
Reports & Memoranda No. 1950. 1*s.* (1*s.* 2*d.*)

Prices in brackets include postage.

Obtainable from

His Majesty's Stationery Office

London W.C.2: York House, Kingsway
[Post Orders—P.O. Box No. 569, London, S.E.1.]
Edinburgh 2: 13A Castle Street
Manchester 2: 39-41 King Street
Cardiff: 1 St. Andrew's Crescent
Bristol 1: Tower Lane
Belfast: 80 Chichester Street
or through any bookseller.

S.O. Code No. 23-2165